Kinetic electron and ion instability of the lunar wake simulated at physical mass ratio

Citation: Haakonsen, Christian Bernt, Ian H. Hutchinson, and Chuteng Zhou. "Kinetic Electron and Ion Instability of the Lunar Wake Simulated at Physical Mass Ratio." Physics of Plasmas 22.3 (2015): 32311.

As Published: http://dx.doi.org/10.1063/1.4915525

Publisher: American Institute of Physics (AIP)

Persistent URL: http://hdl.handle.net/1721.1/104933

Version: Author's final manuscript: final author's manuscript post peer review, without publisher's formatting or copy editing

Kinetic Electron and Ion Instability of the Lunar Wake Simulated at Physical Mass Ratio

Christian Bernt Haakonsen,[1, a)] Ian H. Hutchinson,[1, b)] and Chuteng Zhou[1, c)]
Plasma Science and Fusion Center, Massachusetts Institute of Technology

(Dated: 25 February 2015)

The solar wind wake behind the moon is studied with 1D electrostatic particle-in-cell (PIC) simulations using a physical ion to electron mass ratio (unlike prior investigations); the simulations also apply more generally to supersonic flow of dense magnetized plasma past non-magnetic objects. A hybrid electrostatic Boltzmann electron treatment is first used to investigate the ion stability in the absence of kinetic electron effects, showing that the ions are two-stream unstable for downstream wake distances (in lunar radii) greater than about three times the solar wind Mach number. Simulations with PIC electrons are then used to show that kinetic electron effects can lead to disruption of the ion beams at least three times closer to the moon than in the hybrid simulations. This disruption occurs as the result of a novel wake phenomenon: the non-linear growth of electron holes spawned from a narrow dimple in the electron velocity distribution. Most of the holes arising from the dimple are small and quickly leave the wake, approximately following the unperturbed electron phase-space trajectories, but some holes originating near the center of the wake remain and grow large enough to trigger disruption of the ion beams. Non-linear kinetic-electron effects are therefore essential to a comprehensive understanding of the 1D electrostatic stability of such wakes, and possible observational signatures in ARTEMIS data from the lunar wake are discussed.

PACS numbers: 52.30.-q, 52.35.Fp, 52.35.Mw, 52.35.Qz, 52.35.Qz, 52.35.Sb, 52.35.Tc, 52.65.Rr, 95.30.Qd, 96.20.-n, 96.25.Qr, 96.25.St, 96.50.Ci

I. INTRODUCTION

The supersonic flow of the solar wind past the moon and other objects without global magnetospheres is a topic of continued theoretical and experimental interest. The ongoing ARTEMIS mission[1] is studying the solar wind in the vicinity of the moon, with targeted 3D hybrid simulations being used[2] to interpret the observed fluctuations[3]. More generally, simulations of dense magnetized plasma flow past non-magnetic objects has wide applicability, ranging from probes in laboratory plasmas to asteroids and the moons of Saturn[4,5].

Solar wind flow past the moon leads to an elaborate lunar plasma environment and wake[6]. At distances beyond a few lunar radii the main dynamics of interest are those associated with the ambipolar plasma expansion into the void trailing the moon, and in particular any resulting instabilities. This process has been studied with fully kinetic simulations in 1D[7–9] and 2D[10], as well as with hybrid simulations in 1D[11], 2D[12], and 3D[2,13–15]. There are also 2D kinetic simulations which ignore the magnetic field of the solar wind[16,17], but these are less relevant to the moon given its large size relative to the gyroradius scales in the solar wind.

Despite the wide range of prior simulations, none have so far accurately captured the 1D electrostatic phenomena which can occur in the wakes of large non-magnetic objects. Birch and Chapman[9] attributed the fluctuations they (and previously Farrell et al.[7]) observed to electron beam instability. However, Hutchinson[18] showed that the unphysical ion to electron mass ratio used in those simulations artificially enhances the energy scale of electron–electron instability, indicating that a realistic mass ratio is needed to accurately model such instabilities in the wake. The present work confirms the importance of using a realistic mass ratio, discovering a novel wake phenomenon where electron holes grow from the small energy scale of the electron–electron instabilities to a scale where they can disrupt the counterstreaming ion beams in the wake. This observation has already inspired theoretical investigations into the underlying mechanism[19], which show that the changing density in the wake can act as a drive for hole growth.

Kinetic electron effects are thus shown to be important in the flow of magnetized plasmas past objects much larger than the plasma Debye length. The case of supersonic flow is treated here, but the failure of Boltzmann or other hybrid electron treatments to capture the relevant electrostatic phenomena may well extend to cases with slower plasma flow: counterstreaming ions will also be present for slower flow, and the electrons will still see a varying potential and local density, so the main differences are geometrical and related to boundary conditions at the collecting object. Whether these differences are enough to render the kinetic electron effects unimportant is a topic that should be investigated, as it may be relevant to Mach probes and other means of invasive plasma measurements.

This paper is organized as follows: The 1D electrostatic simulation approach used is described in Section II.

[a)] chaako@mit.edu
[b)] ihutch@mit.edu
[c)] ctzhou@mit.edu

Simulations using Boltzmann electrons are presented in Section III, showing the onset of ion two-stream instability; the unstable (but mass-ratio dependent) electron distributions associated with the Boltzmann-simulated wake are also illustrated. Fully kinetic simulations are presented in Section IV, where some of the electron holes formed early in the wake are seen to grow and lead to disruption of the ion beams much closer to the moon than in the Boltzmann-electron simulations. Possible observational signatures of electron holes and ion-beam disruption in ARTEMIS data are discussed in Section V, and some concluding remarks given in Section VI.

II. 1D ELECTROSTATIC SIMULATION METHOD

The lunar wake simulation is reduced to 1D through the same approach taken in prior such studies[7–9]: by following the plasma in the frame moving with the solar wind, where the perpendicular motion is restricted by the magnetic field. What is simulated is then the parallel motion of electrons and ions along an unperturbed magnetic field line as a function of time. For a static wake this time-dependence can be translated to a spatial dependence by following the trajectory of the field line, and a single 1D simulation thus applies to a wide range of solar wind flow velocities and magnetic field orientations with respect to the moon[18] (in suitably scaled coordinates).

For ease of comparison with the prior studies[7–9] the relative motion of the solar wind and the moon is taken to be perpendicular to the magnetic field and have speed $v_{\rm sw} = 25c_{\rm s}$. Here $c_{\rm s} = \sqrt{T_{\rm e}/m_{\rm i}}$ is the (cold ion) sound speed, which is equal to the ion thermal velocity since $T_{\rm e} = T_{\rm i}$. The distance behind the moon is thus $x = v_{\rm sw}t$, and the position parallel to the magnetic field is denoted y. The particular choice of solar wind speed does not enter into the simulations, only the representation of the results in the figures, so other speeds can be accommodated by a simple scaling of x. Note that the convention for x used herein differs from that used in References 18 and 19 by a factor of the (cold ion) Mach number $v_{\rm sw}/c_{\rm s} = 25$.

A 1D electrostatic particle-in-cell (PIC) code, referred to here as ESPIC, has been developed to carry out the simulations. The ions and electrons are evolved with a standard leap-frog scheme at time steps small enough to resolve the electron motion, and their charge distributed to the two adjacent nodes of the mesh using the cloud-in-cell approach[20]. At each time-step the finite-difference Poisson equation is solved for the potential using a direct tridiagonal method, yielding a constant electric field between any two mesh nodes to accelerate the particles. The potential at the boundaries is set to zero with homogeneous Dirichlet boundary conditions, and particles are injected there according to the assumed Maxwellian background distributions.

ESPIC can be run in parallel to accommodate the large number of particles and time-steps needed to resolve the wide ranges of relevant length and time scales. Even so, large scale-separations such as in the case of the lunar wake present a challenge: the lunar radius $R_{\rm M}$ is 1730 km, while the ion thermal gyroradius is around 40 km and the electron and ion Debye lengths are around 7 m[21,22]. To resolve the Debye length in a domain many lunar radii across would thus require $\sim 10^7$ grid-points, allowing for a few grid-points per Debye length to reduce discretization error. That is not currently feasible using a realistic ion to electron mass ratio, but extrapolation based on simulations at larger (but still small) Debye lengths can yield insight.

For such 1D electrostatic simulations to be applicable, the main influence of the magnetic field on the particles must be to restrict their motion in the directions perpendicular to it. Further, the collecting object (e.g., the moon) must have small apparent extent in the direction of flow, such that the ions do not move much as the field line traverses the object. This can either be because the flow is sufficiently supersonic or because the object has a large aspect ratio, and in either case the detailed shape of the object doesn't matter; its main influence is to leave a region depleted of plasma behind it. The parallel dynamics of the ambipolar plasma expansion into that depleted region then dominate the solution, and can be captured in a 1D domain by suddenly removing the ions and electrons from the part of that domain crossed by the object; this is the approach taken in ESPIC.

Despite not directly influencing the ions, the shape (and surface charge) of the object could still affect the (much faster) electrons. For example, in the case of the lunar wake the electron thermal speed is faster than the solar wind flow (for a realistic mass ratio), so it is not very accurate to model the passage of the moon by a sudden removal of electrons. However, the simultaneous removal of both species provides a convenient way to remove an equal number of electrons and ions, which avoids unphysical charge build-up associated with inaccurate object boundary conditions (especially important for simulations with short Debye length). Further, as will be shown in Section III, the initial electron disturbance (and thus any inaccuracy associated with it) quickly propagates out of the domain in simulations with a realistic mass ratio. Thus, the way of implementing the (2D) passage of the moon in the 1D ESPIC simulations is thought to accurately capture the relevant effects on the part of the wake of interest in the present work.

The main differences between the ESPIC simulations and prior 1D kinetic simulations[7–9] are finer phase-space resolution (up to 2×10^4 grid points and 10^9 particles), the use of a physical mass ratio, and the absence of periodic boundary conditions. Preventing the wake from interacting with itself through the periodic boundaries set a lower limit on the domain size in the prior simulations, and for a physical mass ratio that constraint would be unmanageable. Care must still be taken to avoid reflection of potential structures from the boundaries, but that is much less restrictive in terms of domain size than

the periodic boundaries; if need be absorbing potential boundary conditions could be added allow even smaller domains.

For small Debye length λ_D, a random initialization of particles in the PIC method yields unphysically large fluctuations in the initial potential. This is especially true at long wave-lengths, as the amplitude of potential fluctuations of wavelength λ can be shown to scale with $(\lambda/\lambda_D)^{3/2}$ for Gaussian counting statistics. For the same number of particles, the amplitude of the potential fluctuations can be dramatically reduced by using a *quiet start*[20], where particle positions and velocities are initialized more uniformly than in a true random start; a quiet start is used in ESPIC.

III. BOLTZMANN ELECTRON SIMULATIONS

Hybrid simulation approaches involve the use fluid or other non-kinetic treatments of electrons to greatly reduce the computational cost of simulations, which then only need to resolve the ion time-scales as opposed to the (typically much shorter) electron ones. One such approach is to assume that the electron density along a magnetic field line satisfies a Boltzmann relation

$$n_e = n_{e0} \exp\left(\frac{e\phi}{T_e}\right), \tag{1}$$

which (for instance) it would exactly along a static, monotonically decreasing (repulsive) potential ϕ from some point with a stationary Maxwellian electron distribution of density n_{e0}. Such *Boltzmann electrons* are implemented in ESPIC by solving the non-linear Poisson equation arising from using Equation 1 for the electron density, and are used in the simulations throughout this section (even when moving electrons kinetically to examine their distribution).

The wake structure resulting from a simulation with Boltzmann electrons and a solar wind electron Debye length $\lambda_{De} = 0.02R_M$ is shown in Figure 1. As discussed in Section II a solar wind speed $v_{sw} = 25c_s$ is used to facilitate comparison with prior 1D kinetic simulations[7–9]. The Boltzmann-electron simulation captures the main features of the initial plasma expansion into the void behind the moon seen in the prior simulations: A negative potential in the density-depleted region approximately balances the electron and ion densities, with significant charge density seen only in the transition from unperturbed plasma to the strongly density-depleted region. Later in the wake, for $x \gtrsim 140R_M$, the simulation shows rapid ion (and charge) density variations (vertically elongated striations in the plots) resulting from ion two-stream instability (sometimes referred to as the ion–ion [acoustic] instability[23,24]).

Figure 2 shows the ion phase space for the Boltzmann-electron simulation at three different times/positions. The main initial response of the ions is that they are accelerated towards the void by the negative potential structure. Later in the wake free-streaming of ions is the dominant process, distorting the initial phase space void such that the density-depletion is shallower but more spread out. This sets up a configuration of two ion beams across most of the wake, and the velocity gap between the two beams gradually shrinks. Eventually the the ion two-stream instability grows to a non-linear stage, where large ion holes form and give rise to the ion density variations seen in Figure 1.

Simulations with shorter Debye length show instability-related density variations earlier in the wake, as can be seen in Figure 3. The large-scale structure of the wake is not sensitive to the change in Debye length, so the earlier appearance of the non-linear features of the two-stream instability is caused mainly by the faster growth associated with the higher plasma frequency at shorter Debye length; it takes a significant time for unstable perturbations to grow large enough to be visible when the Debye length is not infinitesimal. Extrapolating to very small Debye-lengths indicates that the ion beams become two-stream unstable when $t \approx 3R_M/c_s$, which corresponds to a distance of $\sim 75R_M$ behind the moon for the particular solar wind speed used in the figures.

Traditionally, Maxwellian beams are considered when studying the two-stream instability (e.g., Ref. 23), and cold ion beams are found to be unstable when their separation is less than about twice the sound speed. However, as illustrated in Figure 4 the ion beams in the simulated wake are not Maxwellian, and have sharp edges associated with the initial void. To include enough particles to resolve the fine features in velocity-space, large spatial bins of width $4\lambda_{De}$ are used when storing the distributions for the following stability analysis, leading to a small amount of smoothing.

The electrostatic ion stability at each location in the wake has been analyzed by calculating numerically the complex Fourier-transformed susceptibility of the (slightly further smoothed) ion distribution at that location together with Maxwellian electrons, in a 1D linearized Vlasov–Poisson system, and setting it equal to zero. The ion–electron instability is suppressed in this calculation by artificially setting the imaginary part of the electron susceptibility to zero; this is appropriate because a Boltzmann electron treatment excludes electron Landau damping or growth. Important deviations of the electron distribution from a Maxwellian will be discussed later, but are not considered here as attention is restricted to the ion two-stream instability. The growth rate γ of the most unstable mode at each location is shown in Figure 5, which clearly supports the interpretation of Figure 3 and the inferred instability onset. The position chosen for the example distribution in Figure 4 can be seen to lie close to the boundary between stable and unstable distributions.

If the imaginary part of the electron susceptibility is included, weak ion–electron instability appears across most

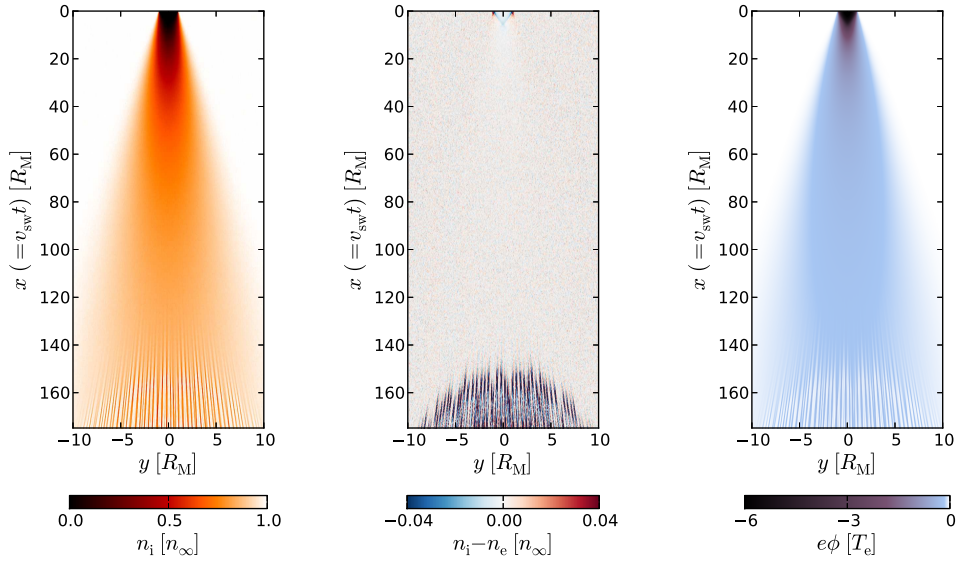

FIG. 1. Ion density $n_{\rm i}$ (in units of solar wind density n_∞), normalized charge density $n_{\rm i}-n_{\rm e}$, and potential ϕ of the wake simulated with Boltzmann electrons for $\lambda_{\rm De}=0.02R_{\rm M}$ (with the illustrative plasma flow speed $v_{\rm sw}=25c_{\rm s}$).

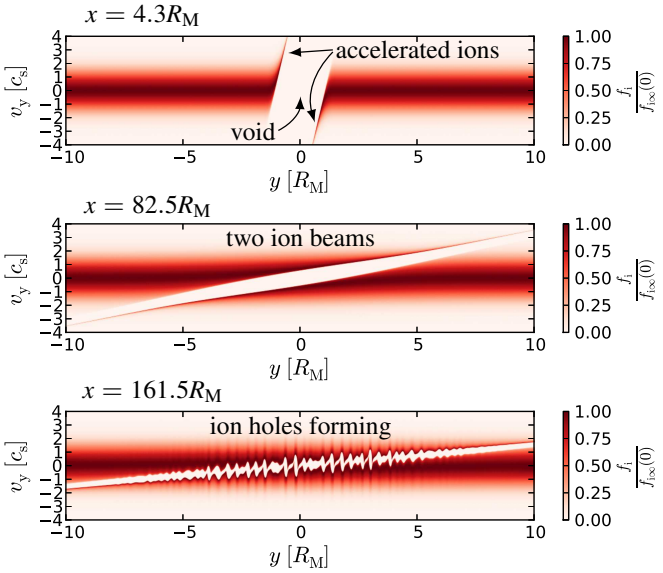

FIG. 2. Ion distribution at three different times (and thus x) in the simulation shown in Figure 1.

of the wake. This instability is likely associated with the sharp edges of the ion beams, and appears to be the instability discussed by Farrell et al.[25] The Boltzmann-electron simulations of this section do not capture that instability, but even in the fully kinetic simulations in Section IV it does not appear to play a large role.

Before moving to fully kinetic simulations, it is useful to examine the electron distributions that arise from the potentials of the Boltzmann-electron simulations. Hutchinson[18] showed that for a model potential evolution the electron distribution develops an unstable depression (a *dimple*) at a position-dependent velocity. Such a dimple is indeed seen in the electron distributions from the Boltzmann-electron simulations, examples of which are shown in Figure 6. The dimple is more pronounced for more artificial mass ratios, leading Birch & Chapman[9] to treat the electron distribution as two electron beams in their stability analysis for $m_{\rm i}/m_{\rm e}=20$. For a realistic mass ratio the dimple only affects a very narrow velocity range of an otherwise largely Maxwellian electron distribution, so treating the distribution as two beams is not appropriate. Also seen in Figure 6 is the initial disturbance to the electron distribution from the (somewhat unphysical) sudden removal of electrons from the computational domain. The disturbance propagates out of the domain very quickly at realistic mass ratios, so any inaccuracy associated with the 1D treatment of the passage of the moon is unlikely to affect the parts of the wake of interest in the present work.

IV. FULLY KINETIC SIMULATIONS

Protons are 1836 times more massive than electrons, providing a lower bound for the true ion to electron mass ratio $m_{\rm i}/m_{\rm e}$ in a typical plasma. Simulations run at such mass ratios are computationally expensive, so a common approach is to use an unphysically small mass ratio in an attempt to capture the essential physics of the scale separation without paying the full computational cost. This was done in prior PIC simulations of the lunar wake[7–10], which used the highly unphysical mass ratio $m_{\rm i}/m_{\rm e}=20$. Later, Hutchinson[18] showed that an unphysical mass ratio greatly enhances the degree to which the lunar wake electron distribution is unstable, and Hong et al.[26] showed that an unphysical mass ratio can significantly affect ion-driven beam instabilities in ways that

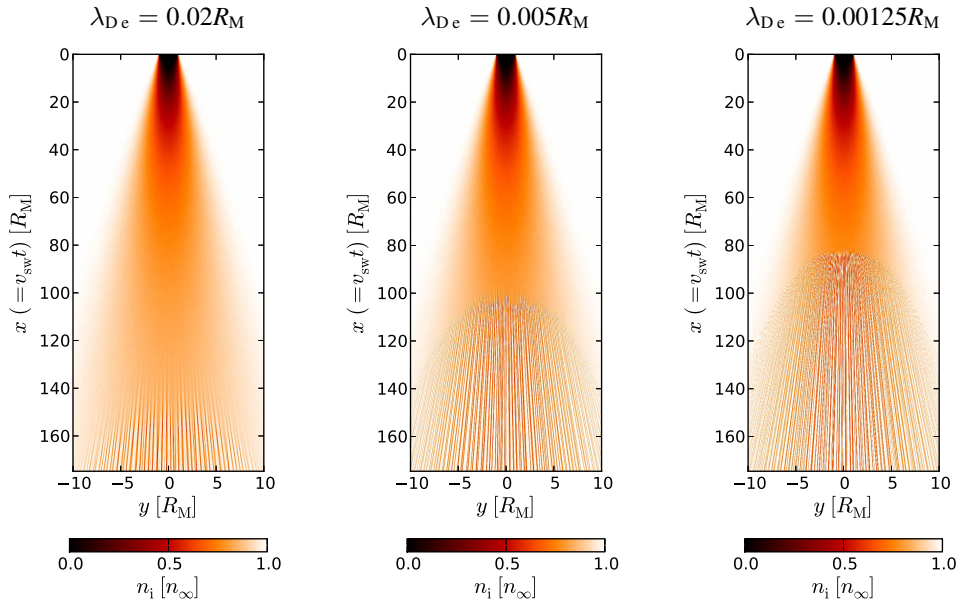

FIG. 3. Ion density in the wake for Boltzmann-electron simulations at three different λ_{De}.

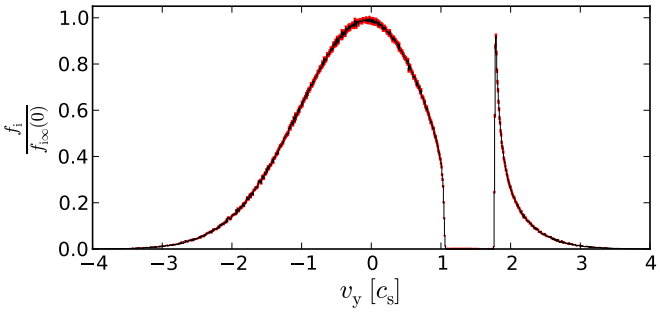

FIG. 4. Ion distribution at $x = 82.5R_M$ and $y = 5R_M$ in Figure 2, with Gaussian counting errors for each bin shown in red.

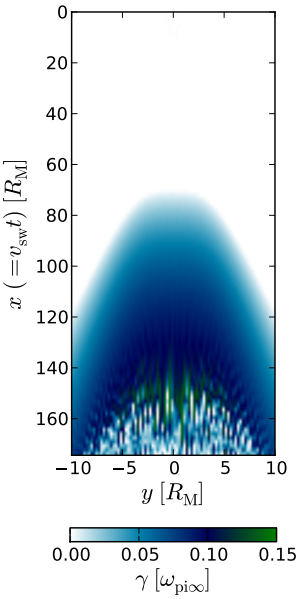

FIG. 5. Maximum linear ion-instability growth rate in wake for simulation shown in Figure 1, in units of the solar wind ion plasma frequency $\omega_{pi\infty}$.

are not easily scaled to a physical mass ratio. Acknowledging these findings, the present work uses simulations at unphysical mass ratios only to illustrate phenomena observed in simulations using the physical mass ratio for hydrogen.

At the true mass ratio and $\lambda_{De} = 0.0025R_M$, treating both electrons and ions kinetically in ESPIC gives rise to the ion density shown in Figure 7. Treating the electrons kinetically gives rise to instability much earlier than was seen in the simulations with Boltzmann electrons (cf. Figure 3). Non-linear disruption of the ion beams in this case occurs at $t \approx 1.1{}^{R_M}/_{c_s}$, which corresponds to a distance of $\sim 28R_M$ behind the moon (at the particular solar wind speed used for illustration). The nature of the density variations is also different, with fewer, less periodic density enhancements gradually widening.

For the same simulation, the evolution of the electron distribution is shown in Figure 8. Very early in the wake, the only noticeable features are the initial void and the (faint) outward propagating initial disturbance from the sudden removal of electrons. Later in the wake a narrow dimple is seen, showing that the dimple persists in some form also when self-consistently considering electron instabilities (cf. Figure 6). Eventually, electron holes with large velocity extent form and gradually widen in spatial extent, corresponding to the density enhancements seen in Figure 7.

Because simulations at the true mass ratio have an extremely narrow dimple and are somewhat noisy, a sim-

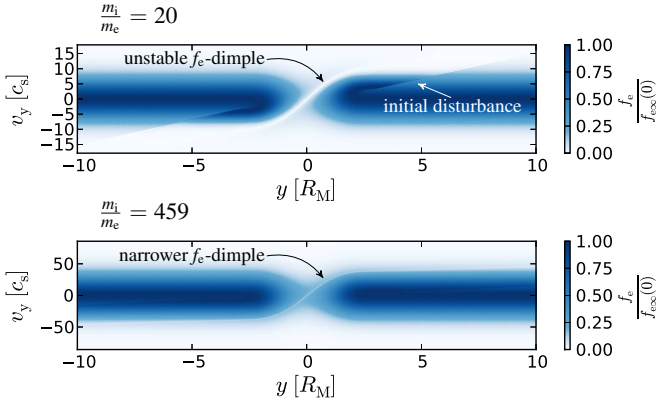

FIG. 6. Electron distribution from potential evolution in Boltzmann-electron simulation, at time corresponding to $x = 15R_M$, for two different mass ratios.

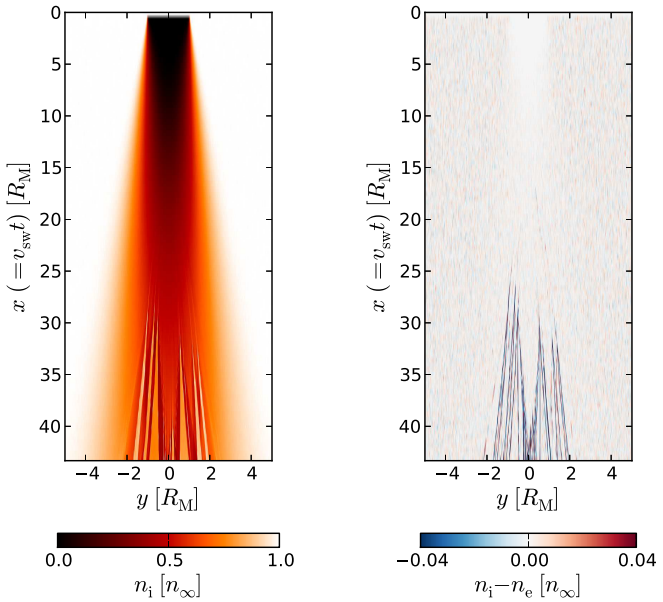

FIG. 7. Ion density n_i and normalized charge density $n_i - n_e$ of wake simulated with kinetic electrons for $\lambda_{De} = 0.0025R_M$.

ulation using $^{m_i}/_{m_e} = 459$ (but the same Debye length) is now used to illustrate the relevant electron phenomena. To better visualize the dimple and holes, a Maxwellian of the same density (and the solar wind electron temperature) is subtracted from the electron distribution at each point in space. The result is shown in Figure 9, for a time before electron holes with large velocity-extent develop. Small hole-like perturbations are seen along the dimple in the electron distribution, and examining consecutive time-steps reveals that they convect outwards along the dimple in phase space (without significantly perturbing the ions).

At a slightly later time, an almost stationary electron hole near $y = 0$ starts growing in velocity extent; the hole moves slowly ($v_y \sim -c_s$) towards negative y, not appearing to accelerate to follow the dimple like the other

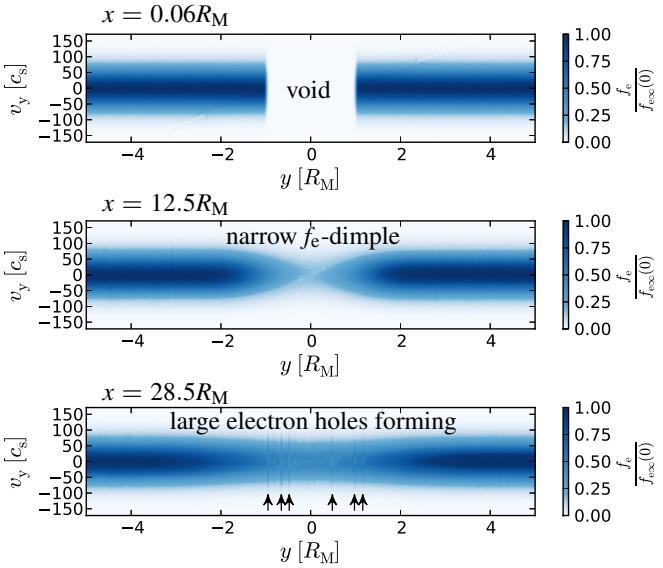

FIG. 8. Electron distribution at three different times (and thus x) in the simulation shown in Figure 7.

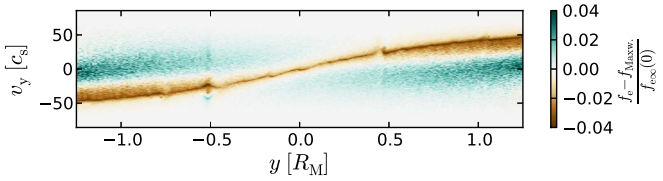

FIG. 9. Departure of electron distribution from a Maxwellian for a simulation with $^{m_i}/_{m_e} = 459$ and $\lambda_{De} = 0.0025R_M$.

holes. The ion and electron distributions in the central region of the domain are shown in Figure 10, for a time when the hole has grown to a large enough extent to significantly perturb the ion beams. After that time the ion beams are quickly disrupted (similarly to in prior simulations[7,9]), further widening the electron hole in velocity as the gap between the ion beams closes. A mechanism has been proposed to explain the growth of such

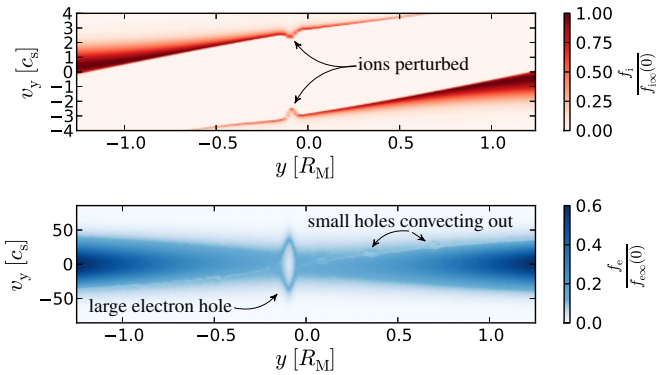

FIG. 10. Ion and electron distributions at a somewhat later time than in Figure 9.

holes[19], whereby the increasing local density as the hole moves downstream drives an expansion of its velocity-extent.

Returning to the simulation at the true mass ratio, a careful examination of the evolution of the electron distribution reveals that the large electron holes seen in Figure 8 arise in the same way as the one discussed for the slightly reduced mass ratio: small holes emerge from the dimple near $y = 0$, move slowly away from the dimple while growing in velocity-extent and remaining centered at small v_y, and then eventually expand to their full velocity-extent as they disrupt the ion beams; the holes then keep expanding in spatial extent as seen in Figure 7. The first seed of a large hole emerges at a time corresponding to $x \approx 14R_M$, where the local electron density is $0.21n_\infty$, and the holes grow until they disrupt the ions around $x = 28R_M$, at which point the local density is in the range $0.46n_\infty$ to $0.56n_\infty$ (depending on the hole position). For the same time-interval the total velocity-separation of the ion beams shrinks from $\sim 5c_s$ to $\sim 3c_s$. That density increase and beam-separation decrease is sufficient for the proposed hole growth mechanism[19] to lead to ion-beam disruption, consistent with the simulations.

Because the electron holes do not remain exactly at $y = 0$ the ion beams are not quite balanced, as illustrated in the (extreme) example in Figure 4. Further, the finite velocities of the electron holes mean that they are likely closer to one of the beams in velocity than to the other, and those velocity-separations evolve as time passes. The situation in the simulations is thus not quite that of the symmetric cold beams considered in the proposed hole growth mechanism[19], but the theory nonetheless seems to capture the main features of the hole growth and beam disruption. Where in the wake the ion beams are disrupted thus depends on two main factors: the amount of electron hole growth from the increasing local density, and the decreasing hole size needed to disrupt the ion beams as their velocity-separation shrinks.

Further simulations have been carried out to explore the sensitivity of the ion-beam disruption to changes in mass ratio and electron Debye length. In general, decreasing the Debye length or the ion to electron mass ratio leads to earlier disruption of the ion beams. For example, changing the mass ratio to $m_i/m_e = 115$ leads to the ion beams being disrupted at a time corresponding to $x \approx 12R_M$, when they are separated by $\sim 5.5c_s$. It is presently not computationally feasible to do true mass ratio simulations with ESPIC at Debye lengths much smaller than the $\lambda_{De} = 0.0025R_M$ of the simulations presented in this section, so the $\lambda_{De} \sim 10^{-5}R_M$ of the solar wind remains out of reach. However, the observed trend is for there to be more electron holes at shorter Debye lengths, appearing and disrupting the ion beams even earlier in the wake; at $\lambda_{De} = 0.00125R_M$ disruption occurs at $x \approx 20R_M$.

V. OBSERVATIONAL SIGNATURES

The ARTEMIS mission[1] has been observing the lunar wake for several years, and a number of potentially relevant observations have been presented[2,3,27,28]. Solar wind variablitity and short Debye lengths in the wake make direct comparisons with the simulations difficult, but a qualitative discussion of possible observational signatures of electron holes and ion-beam disruption is given in this section.

Small electron holes convecting along the dimple in phase space are one of the two main kinetic phenomena observed in the simulations; the holes arise because the dimple is unstable[18], and may be present throughout most of the observed wake. Since the holes remain close to the dimple in phase space their propagation speeds are of order the electron thermal speed (except very close to the center of the wake), and the associated pertubations extend $\lesssim 10\lambda_{De}$ in space (parallel to the magnetic field) and $\lesssim T_e/20e$ in potential. Such a hole may thus for instance extend 100 m along the magnetic field, be moving with a parallel speed of 10^6 m/s, and have a potential amplitude of 0.5 V. That would give an electric field signal of ~ 10 mV/m with duration ~ 0.1 ms, which though weaker and faster than those of electron holes observed in the Earth's plasma sheet[29,30] may still be detectable with ARTEMIS. High-frequency electrostatic fluctuations have been observed in the lunar wake[27], and could in principle be poorly resolved electron holes.

The other main kinetic phenomenon in the simulations is slow-moving electron holes that grow large enough to disrupt the ion beams; their typical propagation speeds are of order the sound speed, their potential pertubations are $\sim T_e/e$, and there is no clear upper limit on their sizes. Such holes may be present beyond a certain distance behind the moon, which depends on the (variable) solar wind parameters but is expected to fall within the range covered by ARTEMIS. Since the ion-disrupting electron holes are slower and perhaps more extended than the small fast holes, their temporal signatures should be of significantly longer durations. That could make them easier to detect and characterise, but may also make them more difficult to disentangle from other signal variations. One of the high-resolution observations reported by Tao et al.[27] revealed broad-band electrostatic fluctuations at around the ion plasma frequency, for which electron holes were proposed as one possible cause (cf. Ref. 31). Though no well-defined solitary structures were identified, the fluctuations could be a sign of ion-disrupting holes, or perhaps of small holes spawned close enough to the center of the wake to be slow.

Halekas et al.[3] presented wake-scale data for the same traversal studied by Tao et al. Ubiquitous ion-disrupting holes could in principle affect the ion distribution even at that scale, but the extent to which such holes could have developed only $\sim 3.5R_M$ downstream of the moon is not known from the simulations. The observed ion spectro-

gram is dominated by the solar wind flow, but does show signs of counterstreaming ions. A higher-resolution segment (Figure 4 of Ref. 3) could be interpreted as showing the gap between the ion beams closing (the beams being disrupted) in some regions, but solar wind variability makes direct interpretation difficult[2]. That the regions with signs of ion-beam disruption lie close to the center of the wake is suggestive, however, since that is where the seeds of the ion-disrupting holes originate in the simulations. It is also where the high-resolution data showed possible signs of slow-moving electron holes[27], and appears to be the source of an outward-propagating electron beam[3]; electron holes generally increase the parallel electron temperature, and deep ones can appear as beams.

There is now an abundance of ARTEMIS data available, as illustrated by recent work[32] creating a 3D map of the typical large-scale structure of the lunar wake. Possible signs of electron holes have been discussed in this section, but specific searches and detailed analysis of high-resolution data are needed to confirm the presence of such holes in the lunar wake.

VI. CONCLUSIONS

The present work highlights the importance of using a realistic ion to electron mass ratio in 1D simulations of magnetized supersonic wakes behind non-magnetic objects. Doing so has revealed a novel phenomenon where the velocity extents of electron holes grow from the small scale associated with electron–electron instability to one where the holes can significantly perturb the ions. As a result, the dimple in the electron distribution remains important despite its narrow width at realistic mass ratios, acting as a seed of electron holes which eventually disrupt the counterstreaming ion beams in the wake much earlier than in the Boltzmann-electron simulations.

Prior kinetic simulations[9,10] observed strong kinetic electron effects at a highly artificial mass ratio ($m_i/m_e = 20$), but could not establish the importance of those effects at physical mass ratios because of the strong mass-ratio dependence of the dimple[18]. The present results demonstrate unequivocally the importance of kinetic electron effects in electrostatic 1D simulations, thus calling into question the validity of the hybrid simulations frequently used in attempts to explain experimental observations. It is conceivable that other physical effects suppress the kinetic electron effects: for example, magnetic perturbations have been shown to be more important for solar wind flow which is far from perpendicular to the magnetic field[12], and so could in principle interfere with the parallel electron and ion dynamics. Unless such a suppressing mechanism can be identified, however, accounting for kinetic electron effects on ion stability appears to be essential.

Because of the small size of the ion thermal gyroradius compared with the radius of the moon, the 1D treatment is likely resonably accurate for the early large-scale structure of the wake. However, the Debye length is significantly smaller than even the electron thermal gyroradius, so the accuracy of the 1D non-linear instability evolution is less certain. In principle the electrostatic modes present in 1D could couple to electromagnetic modes, possibly at oblique angles, giving the instabilities a multi-dimensional nature and introducing pitch-angle scattering, which could affect the electron dimple. Further, the growing electron holes may not be stable for the true ordering of length scales, possibly interfering with the ability of electron holes to reach the size needed to disrupt the ion beams. Kinetic simulations of higher dimensionality are thus needed, though these will be computationally challenging given the need to use a realistic mass ratio and a short Debye length.

Though the lunar wake has been used as the main example of possible applicability of the present simulations, they solve the general problem of supersonic flow past a non-magnetic object. As such they apply equally well to probes in magnetized plasmas and other large bodies in the solar wind, provided the main assumptions hold. The importance of electron kinetic effects at supersonic flow also raises the question of the extent to which similar phenomena can occur at slower magnetized plasma flow, but to address that question will require multi-dimensional simulations since the finite extent of the object in the flow direction and its boundary conditions then matter.

ACKNOWLEDGMENTS

Useful discussions with David Malaspina regarding electron holes in ARTEMIS data are gratefully acknowledged, as is the anonymous referee for leading us to add Section V. C. B. Haakonsen and C. Zhou were supported by NSF/DOE Grant No. de-sc0010491. Computer simulations using ESPIC were carried out on the MIT PSFC parallel AMD Opteron/Infiniband cluster Loki.

[1] C. Russell and V. Angelopoulos, eds., *The ARTEMIS Mission* (Springer New York, New York, NY, 2014).
[2] S. Wiehle, F. Plaschke, U. Motschmann, K.-H. Glassmeier, H. Auster, V. Angelopoulos, J. Mueller, H. Kriegel, E. Georgescu, J. Halekas, D. Sibeck, and J. McFadden, Planetary and Space Science **59**, 661 (2011).
[3] J. S. Halekas, V. Angelopoulos, D. G. Sibeck, K. K. Khurana, C. T. Russell, G. T. Delory, W. M. Farrell, J. P. McFadden, J. W. Bonnell, D. Larson, R. E. Ergun, F. Plaschke, and K. H. Glassmeier, Space Science Reviews **165**, 93 (2011).
[4] K. K. Khurana, C. Russell, and M. Dougherty, Icarus **193**, 465 (2008).
[5] S. Simon, J. Saur, F. M. Neubauer, U. Motschmann, and M. K. Dougherty, Geophysical Research Letters **36**, L04108 (2009).
[6] J. Halekas, Y. Saito, G. Delory, and W. Farrell, Planetary and Space Science **59**, 1681 (2011).
[7] W. M. Farrell, M. L. Kaiser, J. T. Steinberg, and S. D. Bale, Journal of Geophysical Research **103**, 23653 (1998).
[8] W. M. Farrell, T. J. Stubbs, J. S. Halekas, G. T. Delory, M. R. Collier, R. R. Vondrak, and R. P. Lin, Geophysical Research Letters **35**, L05105 (2008).
[9] P. C. Birch and S. C. Chapman, Physics of Plasmas **8**, 4551 (2001).

[10]P. C. Birch and S. C. Chapman, Physics of Plasmas **9**, 1785 (2002).
[11]P. Israelevich and L. Ofman, Journal of Geophysical Research **117**, A08223 (2012).
[12]P. Trávníček, Geophysical Research Letters **32**, L06102 (2005).
[13]E. Kallio, Geophysical Research Letters **32**, L06107 (2005).
[14]Y.-C. Wang, J. Müller, W.-H. Ip, and U. Motschmann, Icarus **216**, 415 (2011).
[15]M. Holmström, S. Fatemi, Y. Futaana, and H. Nilsson, Earth, Planets and Space **64**, 237 (2012).
[16]P. Guio and H. L. Pécseli, Annales Geophysicae **23**, 853 (2005).
[17]S. Kimura and T. Nakagawa, Earth, Planets and Space **60**, 591 (2008).
[18]I. H. Hutchinson, Journal of Geophysical Research **117**, A03101 (2012).
[19]I. H. Hutchinson, C. B. Haakonsen, and C. Zhou, submitted to Physics of Plasmas (2015).
[20]C. K. Birdsall and A. B. Langdon, *Plasma physics via computer simulation* (Adam Hilger, Bristol, 1991).
[21]K. W. Ogilvie, J. T. Steinberg, R. J. Fitzenreiter, C. J. Owen, A. J. Lazarus, W. M. Farrell, and R. B. Torbert, Geophysical Research Letters **23**, 1255 (1996).
[22]J. S. Halekas, S. D. Bale, D. L. Mitchell, and R. P. Lin, Journal of Geophysical Research **110**, A07222 (2005).
[23]T. E. Stringer, Journal of Nuclear Energy. Part C, Plasma Physics, Accelerators, Thermonuclear Research **6**, 267 (1964).
[24]S. P. Gary and N. Omidi, Journal of Plasma Physics **37**, 45 (1987).
[25]W. M. Farrell, M. L. Kaiser, and J. T. Steinberg, Geophysical Research Letters **24**, 1135 (1997).
[26]J. Hong, E. Lee, K. Min, and G. K. Parks, Physics of Plasmas **19**, 092111 (2012).
[27]J. B. Tao, R. E. Ergun, D. L. Newman, J. S. Halekas, L. Andersson, V. Angelopoulos, J. W. Bonnell, J. P. McFadden, C. M. Cully, H.-U. Auster, K.-H. Glassmeier, D. E. Larson, W. Baumjohann, and M. V. Goldman, Journal of Geophysical Research **117**, A03106 (2012).
[28]J. S. Halekas, A. R. Poppe, and J. P. McFadden, Journal of Geophysical Research: Space Physics **119**, 5133 (2014).
[29]L. Andersson, R. Ergun, J. Tao, A. Roux, O. LeContel, V. Angelopoulos, J. Bonnell, J. McFadden, D. Larson, S. Eriksson, T. Johansson, C. Cully, D. Newman, M. Goldman, K.-H. Glassmeier, and W. Baumjohann, Physical Review Letters **102**, 225004 (2009).
[30]J. B. Tao, R. E. Ergun, L. Andersson, J. W. Bonnell, A. Roux, O. LeContel, V. Angelopoulos, J. P. McFadden, D. E. Larson, C. M. Cully, H.-U. Auster, K.-H. Glassmeier, W. Baumjohann, D. L. Newman, and M. V. Goldman, Journal of Geophysical Research **116**, A11213 (2011).
[31]H. Kojima, H. Matsumoto, S. Chikuba, S. Horiyama, M. Ashour-Abdalla, and R. R. Anderson, Journal of Geophysical Research **102**, 14439 (1997).
[32]H. Zhang, K. K. Khurana, M. G. Kivelson, V. Angelopoulos, W. X. Wan, L. B. Liu, Q.-G. Zong, Z. Y. Pu, Q. Q. Shi, and W. L. Liu, Journal of Geophysical Research: Space Physics **119**, 5220 (2014).